Effects of local hemodynamics and plaque characteristics on neointimal response following bioresorbable scaffolds implantation in coronary bifurcations

Chu, M.; Gutierrez-Chico, J.L.; Li, Y.G.; Holck, E.N.; Zhang, S.; Huang, J.Y.; ... ; Tu, S.X.

The International Journal of Cardiovascular Imaging (2020) 36:241–249
https://doi.org/10.1007/s10554-019-01721-7

ORIGINAL PAPER

Effects of local hemodynamics and plaque characteristics on neointimal response following bioresorbable scaffolds implantation in coronary bifurcations

Miao Chu[1,2] · Juan Luis Gutiérrez-Chico[2] · Yingguang Li[3] · Emil N. Holck[4] · Su Zhang[1] · Jiayue Huang[1] · Zehang Li[1] · Lianglong Chen[5] · Evald H. Christiansen[4] · Jouke Dijkstra[3] · Niels R. Holm[4] · Shengxian Tu[1]

Received: 31 May 2019 / Accepted: 18 October 2019 / Published online: 30 October 2019

Abstract

Heterogeneous neointimal response has been observed after implantation of all generations of coronary stents. Our aim was assessing local factors of shear stress (SS) and plaque characteristics in neointimal response after implantation of bioresorbable scaffolds (BRS) in bifurcations. Ten patients from the BIFSORB pilot study were analysed. Follow-up optical frequency domain imaging (OFDI) was performed at 1 month and 2 years. Coronary lumen and BRS structure were reconstructed by fusion of OFDI and angiography and were used for subsequent flow simulation. Plaque arc degree and SS were quantified using post-procedural OFDI data and were matched with follow-up OFDI using anatomical landmarks. Strut-level and segment-level analysis were performed for 1-month and 2-year follow-up respectively. A total of 444 struts (54 jailing struts) were included at 1-month follow-up. Time-average SS (TASS) was significantly lower for covered struts than for uncovered struts in non-bifurcation segments (TASS: 1.81 ± 1.87 vs. 3.88 ± 3.72 Pa, $p < 0.001$). The trend remained the same for jailing struts, although statistically insignificant (TASS: 10.85 ± 13.12 vs. 13.64 ± 14.48 Pa, $p = 0.328$). For 2-year follow-up, a total of 66 sub-regions were analysed. Neointimal hyperplasia area (NTA) was negatively correlated with TASS in core-segments ($\rho = -0.389$, $p = 0.037$) and positively correlated with plaque arc degree in non-core segments ($\rho = 0.387$, $p = 0.018$). Slightly stronger correlations with NTA were observed when combining TASS and plaque arc degree in both core segments ($\rho = -0.412$, $p = 0.026$) and non-core segments ($\rho = -0.395$, $p = 0.015$). Hemodynamic microenvironment and baseline plaque characteristics may regulate neointimal response after BRS implantation in bifurcation. These findings underline the combined role of plaque characteristics and local hemodynamics in vessel healing after stent implantation.

Keywords Shear stress · Plaque arc degree · Stent healing · Optical coherence tomography

Abbreviations

BMS	Bare metal stents
BRS	Bioresorbable scaffolds
CFD	Computational fluid dynamics
DES	Drug-eluting stents
ISR	In-stent restenosis
IST	In-stent thrombosis
IVUS	Intravascular ultrasound
OFDI	Optical frequency domain imaging
OCT	Optical coherence tomography
PCI	Percutaneous coronary intervention
SB	Side branch
SS	Shear stress
SSG	Shear stress gradient
TASS	Time-average shear stress
TASSG	Time-average shear stress gradient

✉ Shengxian Tu
sxtu@sjtu.edu.cn

1 School of Biomedical Engineering, Shanghai Jiao Tong University, Room 123, No. 1954, Huashan Road, Shanghai 200030, People's Republic of China

2 Department of Cardiology, Campo de Gibraltar Health Trust, Algeciras (Cádiz), Spain

3 Division of Image Processing, Leiden University Medical Center, Leiden, The Netherlands

4 Department of Cardiology, Aarhus University Hospital, Skejby, Denmark

5 Department of Cardiology, Fujian Medical University Union Hospital, Fuzhou, Fujian, China

NTA Neointimal hyperplasia area
NHT Neointimal hyperplasia thickness

Introduction

Percutaneous coronary intervention (PCI) with stent implantation is the standard therapeutic approach to restore blood flow in the downstream myocardium in patients with coronary artery disease, but stent failure can occur at follow-up like in-stent restenosis (ISR) or in-stent thrombosis (IST), thus jeopardising an initially good clinical result. ISR may be caused by neointimal hyperplasia while incomplete strut endothelialization and delayed healing are potential triggers for IST [1]. The advances of intracoronary optical coherence tomography (OCT) enable detailed in vivo evaluation of stent healing processes and heterogeneous neointimal response has been observed after stent implantation [2], indicating that in addition to well-appreciated risk factors, local factors are likely to be involved in the healing processes. Low endothelial shear stress (SS) has been shown to contribute to severe endothelial dysfunction and is associated with increased neointimal thickness after stenting [3, 4]. However, the role of SS at bifurcations has not been elucidated so far. Furthermore, neointimal response is modulated by multiple local factors besides SS including plaque burden and composition [5, 6]. The combined effect of these factors remains unknown. The aim of this study was to investigate the influence of local SS and baseline plaque characteristics on scaffold coverage after bioresorbable vascular scaffolds (BRS) implantation in bifurcations at 1-month and 2-year follow-up.

Methods

Study population

A post hoc analysis of data of the BIFSORB pilot study (NCT02973529) was performed, which has already been described by Holck et al. [7]. In brief, 10 patients indicated for treatment of coronary bifurcation lesion involving a side branches (SB) $\geq$2.5 mm were included. Baseline optical frequency domain imaging (OFDI) was performed during and after implantation of the DESolve BRS (Elixir, USA) using the provisional SB stenting technique, aiming at evaluating the feasibility and self-correcting properties of the scaffold. Follow-up OFDI imaging was performed at 1 month and 2 years. The study was conducted according to the Declaration of Helsinki and was approved by the Central Denmark Region Ethics Committee for Biomedical Research and the Danish Data Protection Agency. All patients provided written informed consent.

Reconstruction of the coronary tree and BRS

The 3D reconstruction of the coronary arteries and implanted BRS was performed by the fusion of OFDI images and coronary angiography using a previously described methodology [8]. In brief, two angiographic image runs with minimal overlap and foreshortening were selected to reconstruct the stented main vessel and its SB > 1 mm diameter by QAngio XA 3D RE (Medis Special bv, the Netherlands) [9]. The contours of both the coronary lumen and implanted scaffolds in the post-procedural OFDI pullback were delineated semi-automatically by QCU-CMS (Leiden University Medical Centre, the Netherlands) [8]. A fused coronary tree was created by combining lumen of the main vessel from OFDI and SB from the angiograms after correcting longitudinal and rotational distortion of OFDI pullback. Finally, scaffold structures were reconstructed in 3D space and subsequently fused with the tree, generating a new lumen tree surface with BRS structures.

Blood flow simulation

Reconstructed models of the coronary artery tree with BRS structure were discretized into unstructured tetrahedral elements with the global element size between 0.02 and 0.2 mm^3 by ICEM 17.0 (ANSYS Inc., Canonsburg, PA, USA). Approximately 0.5 million to 6 million tetrahedral elements were generated per model. Blood flow simulation was performed by solving the Navier–Stokes equation using finite volume method by Fluent 17.0 (ANSYS, Inc.). Newtonian flow with blood density of 1060 kg/m^3 and viscosity of 0.0035 Pa · s was applied. A pulsatile flow waveform with patient specific mean velocity value, which was obtained by combining the dye flow time and coronary tree volume, was imposed at the inlet of the model. Flow separation ratios of SB were determined by bifurcation angles and reference lumen diameter. The artery lumen and BRS surface were considered to be rigid wall and non-slip conditions were applied, whereas fully developed flow conditions were imposed at the outlet of the model. The computations were considered converged when the maximum change in hemodynamic parameters between iterations was < 0.1%. SS at the baseline lumen and stent surface was automatically calculated by CFD-POST (ANSYS, Inc.). Time-average shear stress (TASS) within one cardiac cycle and TASS spatial gradient (TASSG) were derived from the simulation results by MATLAB (The MathWork Inc., Natick, MA) according to the following formulas:

$$TASS = \frac{1}{T}\int_0^T |\overrightarrow{\tau_w}|dt$$

$$SSG = \sqrt{\left(\left|\frac{\partial \overrightarrow{\tau_w}}{\partial x}\right|\right)^2 + \left(\left|\frac{\partial \overrightarrow{\tau_w}}{\partial y}\right|\right)^2 + \left(\left|\frac{\partial \overrightarrow{\tau_w}}{\partial z}\right|\right)^2}$$

$$TASSG = \frac{1}{T}\int_0^T (SSG)dt$$

$\overrightarrow{\tau_w}$: wall shear stress, T: one cardiac cycle, ∂/∂x, ∂/∂y, ∂/∂z: derivation along x, y, z directions respectively, TASS: time-average shear stress, SSG: shear stress gradient, TASSG: time-average shear stress gradient

OCT acquisition and analysis

OCT was acquired using the Lunawave OCT system (Terumo corp, Jp) at a pullback speed of 15 mm/s and a frame rate of 158.00 frames/s during continuous flushing, resulting an interval of 0.095 mm between two consecutive cross-sections. Quantitative OCT analysis was performed in a core laboratory by one experienced analyst. Inspired by van Ditzhuijzen et al. [10], a matching method for the selection of serially corresponding struts and cross sections were employed to avoid distortions caused by the longitudinal motion of OCT catheter. Post-procedural and follow-up OFDI images were matched up according to anatomical landmarks using QCU-CMS. Strut level analysis was performed for one-month follow-up data (Fig. 1a). The analysts identified corresponding struts between baseline and follow-up OFDI examinations with 1-mm frame intervals in non-bifurcated segments and identified all matched struts for all frames located at the SB ostium. Struts where the abluminal surface was detached from the vessel wall were excluded due to the limited fraction of malapposed struts. Neointimal hyperplasia thickness (NHT) was measured as the distance between the ad-luminal stent surface and the lumen contour at follow-up (Fig. 1a). Strut was considered covered if NHT ≥ 35 μm for all sides of struts [11]. Strut coverage was correlated with baseline SS at the corresponding location, with a region of interest of 0.3 mm in length and 0.3 mm in arc-width that assembled twice of the strut size. For 2-year follow-up, segment level analysis was performed for each stented bifurcation (Fig. 1b). Vessels were divided into proximal main vessel, bifurcation core and distal main vessel and were further divided into two sub-regions according to its relative direction with respect to the ostium: opposite and adjacent to the ostium. The observers matched the corresponding sub-segments between baseline and 2-years follow-up OFDI examinations. In order to assess plaque characteristics, plaque components were classified into fibrosis, lipid pool, and calcium according to the established criteria [12]. Fibrous plaque was defined as having high backscattering and a relatively homogeneous OFDI signal. Low OFDI signal with poorly delineated borders and a cap was identified as lipid plaque. Calcium appeared as a signal-poor heterogeneous region with a sharply delineated border. Baseline plaque arc degree, defined as the total circumferential angle of all plaque components in one cross-section, and stent and lumen area at follow-up were measured every 0.2-mm interval. Neointimal hyperplasia area (NHA) was calculated as adluminal scaffold area minus lumen area (Fig. 1b).

Statistical analysis

Continuous variables were tested with the Shapiro–Wilk test for normal distribution and presented as mean ± SD or median (interquartile range) as appropriate. Categorical variables are presented as counts and percentages. Comparison of continuous variables was performed with the independent *t* test or the nonparametric Mann–Whitney's test, depending on the distribution of data. In order to test the potential clustering of arterial segments within patients, null model multi-level analysis was performed to estimate the patient level effect. Spearman correlation coefficient and generalized linear regression analyses were implemented to investigate the association of the baseline SS or the logarithmic transformed SS and plaque arc degree with NHT or NHA at follow-up. Statistical significance was set at the 0.05 level. All statistical analyses were performed with SPSS 19.0 (SPSS Inc., Chicago, IL).

Results

Baseline clinical and lesion characteristics

All ten patients from the BIFSORB pilot study were investigated with OFDI at baseline. Measured by 3D angiography, the mean reference diameter of main vessels was 3.3 ± 0.5 mm at proximal and 2.9 ± 0.3 mm at distal and 2.4 ± 0.3 mm at the SB. Diameter stenosis was 68% in the main vessels and 43% in the ostium of the SB before intervention. Follow-up OFDI at one-month and at 2-year was performed in 8 patients. Six of them were followed-up at both time points. One drug-eluting stent (DES) was implanted on top of the BRS in one patient due to delivery failure. Only the segments with BRS implanted that were not covered by DES were analysed. Figure 2 shows two representative examples of heterogeneous neointimal responds after BRS implantation in this study. The characteristics of the studied population are in Table 1. For further patient and procedural characteristics see publication by Holck et al. [7].

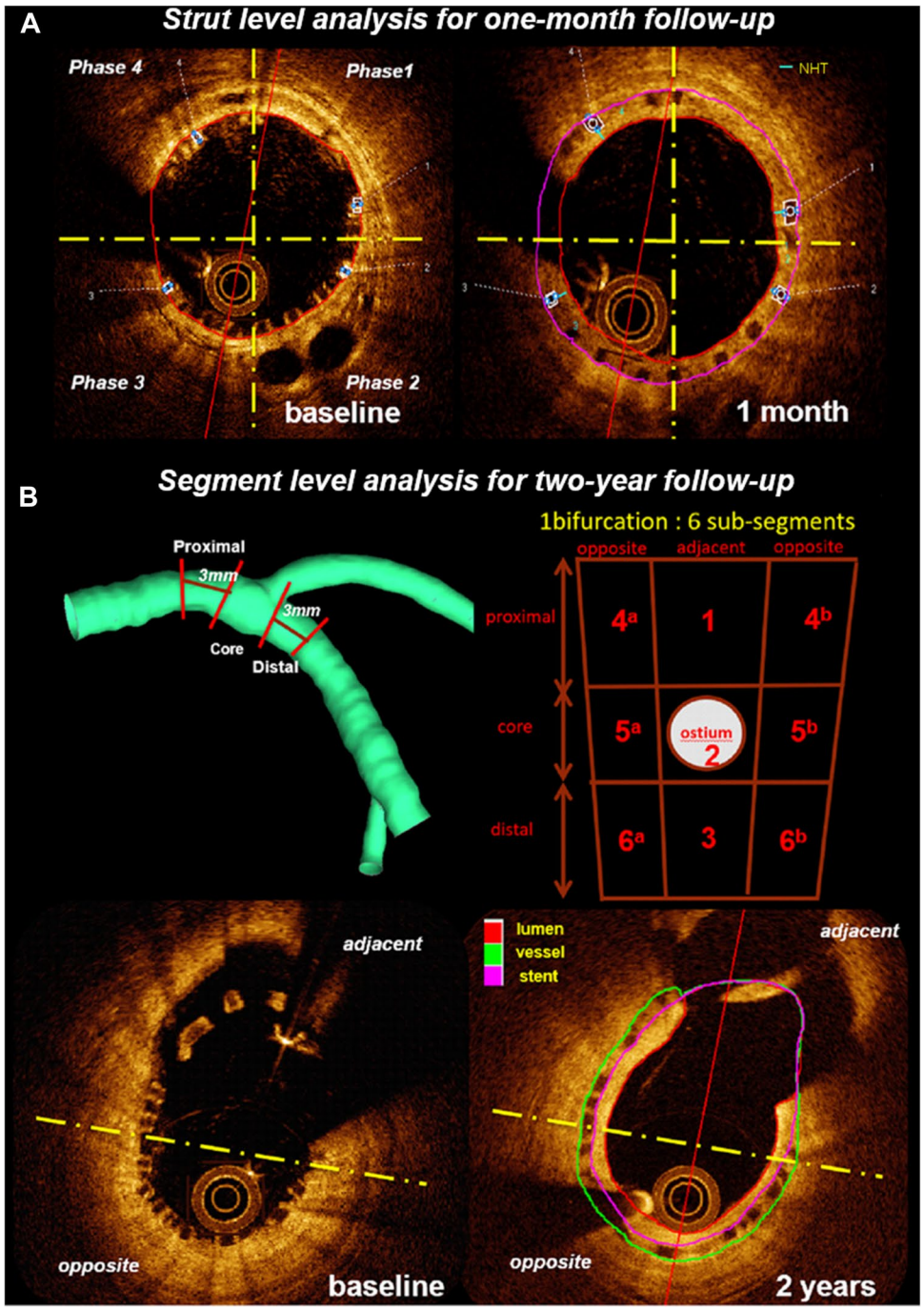

Fig. 1 OCT analysis for one-month and two-year follow-up. **a** Strut level analysis for 1-month follow-up. In non-bifurcated segments, the matched frames of baseline and follow-up were divided into four phases and the most matched strut in each phase was analyzed. All matched jailing struts were included in analysis. **b** Segment level analysis for 2-year follow-up at each stented bifurcation

Multi-level analysis

Null model multi-level analysis was performed on hemodynamic parameters, plaque arc degree and neointimal thickness and area, which turned out that random coefficient of patient subject was statistically insignificant, indicating that there was no interdependence of clustered data on patient level.

Baseline shear stress distribution

A total of 444 struts were analysed for 1-month follow-up and 54 of them were jailing struts. Jailing struts were exposed to significantly higher SS magnitude (2.21 ± 2.48 vs. 11.42 ± 13.31 Pa, $p < 0.001$) and gradients (11.65 ± 12.67 vs. 69.39 ± 75.54 Pa/mm, $p < 0.001$) than struts in non-bifurcation segments (Fig. 3a, b). For 2-year follow-up, a total of 66 sub-regions (20 distal, 29 core and 17 proximal segments) were analysed. In core and distal segments, TASS and

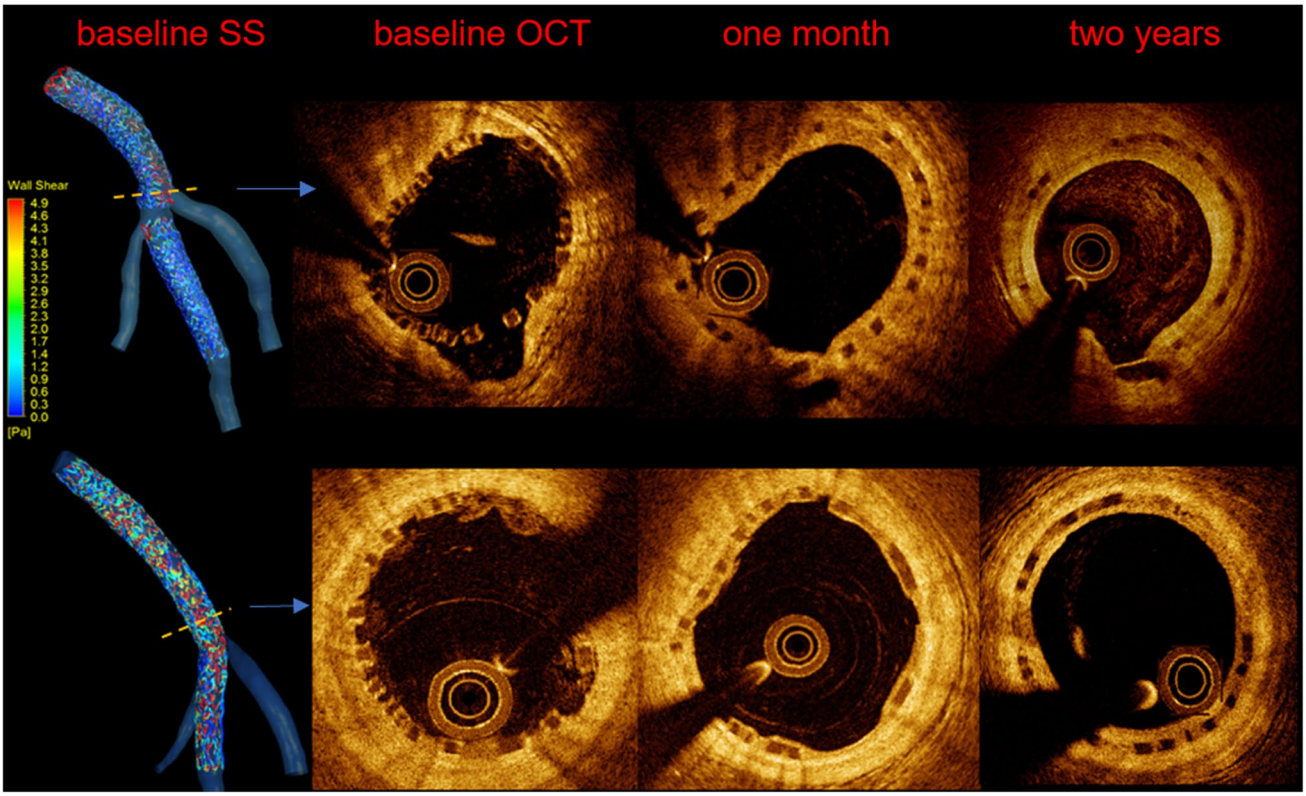

Fig. 2 Heterogenous vascular response after BRS implantation after 1 month and 2 years

TASSG were significantly higher for sub-regions adjacent to the ostium than those opposite to the ostium (Fig. 3c, d).

One-month follow-up

Shear stress at covered and uncovered struts

Forty-three out of 54 jailing struts (79.6%) and 314 out of 390 struts (80.5%) in non-bifurcation segments were covered. TASS and TASSG were significantly lower for covered struts than uncovered struts in non-bifurcation segments (TASS: 1.81 ± 1.87 vs. 3.88 ± 3.72 Pa, $p < 0.001$; TASSG: 9.55 ± 9.45 vs. 20.30 ± 19.12 Pa/mm, $p < 0.001$). The trend remained the same for jailing struts, although statistically insignificant (TASS: 10.85 ± 13.12 vs. 13.64 ± 14.48 Pa, $p = 0.328$; TASSG: 66.71 ± 69.39 vs. 79.87 ± 73.68 Pa/mm, $p = 0.308$). (Figure 3a, b).

Neointimal hyperplasia thickness

The mean NHT was 74.85 ± 34.00 μm for all covered struts at 1-month follow-up. For struts at non-bifurcation, there was a negative weak correlation of NHT with TASS (Spearman rho (ρ) $= -0.165$, $p = 0.003$) and TASSG ($\rho = -0.14$, $p = 0.013$). The generalized linear regression yielded a significant relationship of NHT $= -8.69$*log(TASS) $+73.16$ μm ($p = 0.042$).

Two-year follow-up

Effects of baseline shear stress

The mean NHA was 0.10 ± 0.05 mm^2 at 2 years and the overall correlations of NHA with TASS and TASSG were -0.219 ($p = 0.077$) and -0.191 ($p = 0.125$). When applying generalized linear regression, log(TASS) entered into the model yielding a relationship of NHA $= -0.28$ *log (TASS) $+ 1.12$ mm^2 ($p = 0.015$). The negative correlations of NHA with TASS and TASSG were significant in core sub-segments (TASS: $\rho = -0.389$, $p = 0.037$ and TASSG: $\rho = -0.392$, $p = 0.036$), resulting a significant relationship of NHA $= -0.31$*log(TASS) $+1.16$ mm^2 ($p = 0.010$) and NHA $= -0.30$*log(TASSG) $+1.385$ mm^2 ($p = 0.009$) by generalized linear regression. The correlations were weaker and did not reach statistical significance in non-core segments (Table 2).

Effects of plaque arc degree

The mean plaque arc degree was $80.6 \pm 50.5°$ for all sub-segments. As shown in Table 2, NHA was

Table 1 Baseline clinical characteristics

Age (years)	64 ± 13
BMI (kg/m^2)	26 ± 3
LVEF (%)	57 ± 7
Sex (Male)	8 (80%)
Familiar IHD	6 (60%)
Dyslipidaemia	9 (90%)
Hypertension	4 (40%)
Smoking (active)	5 (50%)
Diabetes	3 (30%)
Previous revascularization (n = 4)	
Previous PCI	3 (30%)
Previous CABG	1 (10%)
Medina classification	
1.1.0	7 (70%)
0.1.0	1 (10%)
1.0.1	1 (10%)
1.1.1	1 (10%)
Target lesion	
LAD/D1	5 (50%)
LAD/D2	2 (20%)
LM	2 (20%)
LCx/OM1	1 (10%)

BMI body mass index, *D1* 1st diagonal branch, *D2* 2nd diagonal branch, *IHD* ischemic heart disease, *LAD* left anterior descending artery, *LCx* left circumflex artery, *LM* left main, *LVEF* left ventricular ejection fraction, *OM1* 1st obtuse marginal branch, *PCI* percutaneous coronary intervention

significantly related with plaque arc degree with a Spearman coefficient of $\rho = 0.285$ ($p = 0.020$) and a relationship of NHA = 0.35*log(Plaque acr) + 0.37 mm^2 ($p = 0.003$). The correlation was stronger in non-core sub-segments with $\rho = 0.387$ ($p = 0.018$) but weaker in core sub-segments with $\rho = 0.116$ ($p = 0.548$).

Interaction of shear stress with plaque arc degree

Two new parameters of *combined_d* = log (TASS/(PlaqueArc + 1)) and *combined_m* = log (TASS*(PlaqueArc + 1)) were generated to explore the interaction between SS and plaque arc degree. As shown in Table 2, the *combined_d* had a significantly higher correlation with NHA both in core sub-segments and non-core sub-segments with $\rho = -0.395$ ($p = 0.015$) and -0.412 ($p = 0.026$). Generalized linear regression yielded significant relationships of NHA = −0.242*log (TASS/(PlaqueArc + 1)) + 0.679 mm^2 ($p = 0.043$) and NHA = −0.278*log (TASS/(PlaqueArc + 1)) + 0.625 mm^2 ($p = 0.021$) for core and non-core sub-segments respectively. There was no significant correlation between *combined_m* and NHA.

Plaque composition

Nine of 66 sub-segments had calcified plaque with a mean arc degree of 34.8 ± 26.6° at baseline. These nine sub-segments had significantly higher NHA and maximum neointimal thickness (NT_max) than those without calcium composition at 2-year follow-up (NHA = 0.95 ± 0.36 and 1.31 ± 0.76 mm^2, $p = 0.045$; NT_max = 0.33 ± 0.08 and 0.42 ± 0.15 mm, $p = 0.012$).

Discussion

The main findings of this study can be summarised as follows: (1) Struts with tissue coverage at 1 month after BRS implantation had lower baseline TASS and TASSG than uncovered struts; (2) NHA at 2 years after BRS implantation was negatively correlated to baseline SS at core segments and positively correlated with baseline plaque arc degree at non-core segments; (3) The combination of baseline SS and plaque arc degree improved the correlation with 2-year NHA in both core and non-core segments.

From a methodological point of view, the current study is original in various aspects. Firstly, this is the first study to correlate neointimal healing processes with baseline shear stress that took the effects of stent structure on blood flow into account. Several studies have previously examined the association between local hemodynamic factors and neointima formation. Wentzel et al. first observed an inverse correlation between baseline SS and neointima formation at 6-month follow-up after bare metal stents (BMS) [13], finding confirmed in subsequent studies [14, 15]. Similar inverse correlations between baseline SS and neointimal thickness at follow-up were also observed after BRS implantation [4]. Inconsistent results have been reported for drug-eluting stents (DES) because the limited neointima formation impeded the evaluation of neointima characteristics [3, 15, 16]. Nonetheless, all previous pioneer studies disregarded the potential role played by the stent structure, particularly when the structure is detached from the vessel wall as with malapposition or jailing struts. Currently compelling evidences have shown how critical stent structure influences flow dynamics [17]. The foreign material protruding into the lumen disturbs laminar flow, and induces flow separation and recirculation locally [18]. Therefore, implementation of a real stent reconstruction in addition to the mere vessel wall is essential for accurate and reliable evaluation of the acting forces.

Secondly, the effects of hemodynamic environments on neointimal healing in bifurcations have been scarcely investigated. In previous stent healing studies, stented segments containing side branch were usually excluded from analysis [4, 13, 19], therefore the role of SS at bifurcations has not been elucidated so far. Following our previously developed

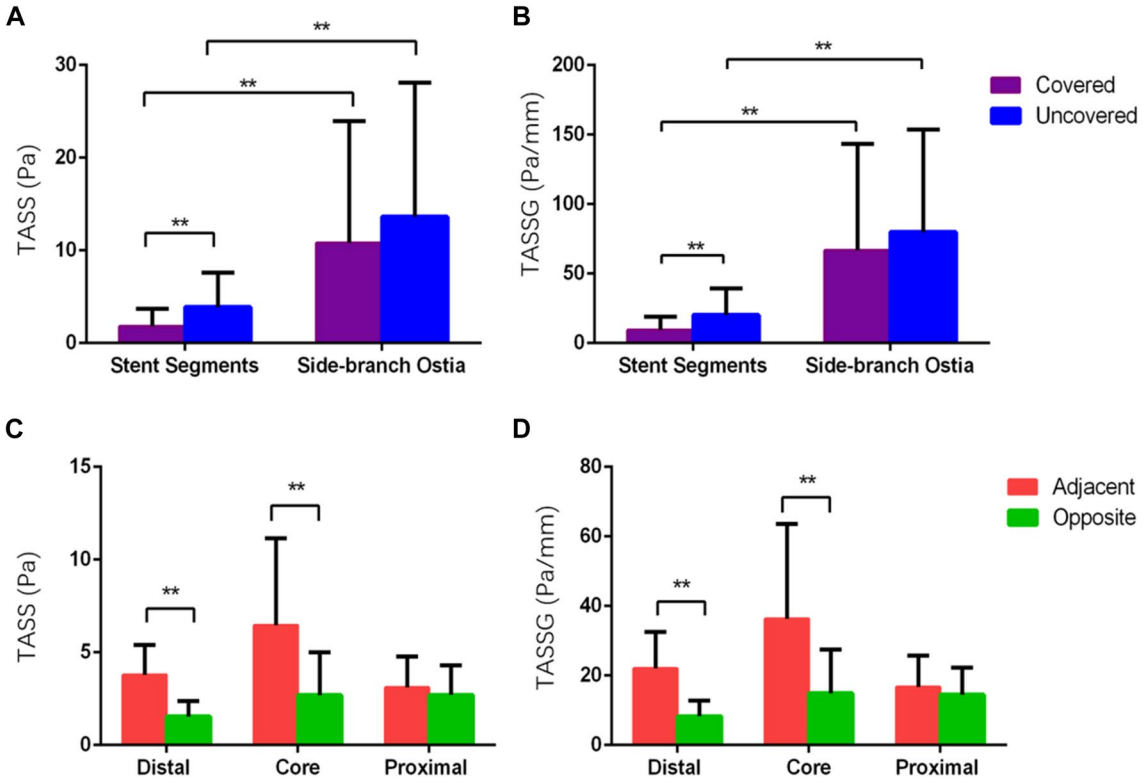

Fig. 3 Shear stress magnitude and gradient distribution. **a**, **b** Jailing struts located at side-branch ostia had higher TASS (2.21 ± 2.48 vs. 11.42 ± 13.31 Pa, $p < 0.001$) and TASSG (11.65 ± 12.67 vs. 69.39 ± 75.54 Pa/mm, $p < 0.001$) than struts in stented segments. TASS and TASSG were lower for covered struts than uncovered struts (TASS: 1.81 ± 1.87 vs. 3.88 ± 3.72 Pa, $p < 0.001$; TASSG: 9.55 ± 9.45 vs. 20.30 ± 19.12 Pa/mm, $p < 0.001$) (C, D) TASS and TASSG were higher for sub-regions adjacent to the ostium than those opposite to ostium. *TASS* time-average shear stress, *TASSG* time-average shear stress gradient

Table 2 Spearman coefficients between local factors and follow-up neointimal response

1 month	TASS (Pa)		TASSG (Pa/mm)			
NHT	ρ	p-Value	ρ	p-Value		
Non-bifurcation (n = 314)	−0.165	0.003	−0.14	0.013		
Jailing sturts (n = 43)	0.049	0.755	0.107	0.496		
2 years	TASS (Pa)		TASSG (Pa/mm)			
NHA	ρ	p-Value	ρ	p-Value		
Core (n = 29)	−0.389	0.037	−0.392	0.036		
Non-core (n = 37)	−0.094	0.58	−0.051	0.762		
All (n = 66)	−0.219	0.077	−0.191	0.125		
2 years	PlaqueArc		Combined_d		Combined_m	
NHA	ρ	p-Value	ρ	p-Value	ρ	p-Value
Core (n = 29)	0.116	0.548	−0.412	0.026	−0.152	0.432
Non-core (n = 37)	0.387	0.018	−0.395	0.015	0.271	0.104
All (n-66)	0.285	0.02	−0.419	< 0.001	0.092	0.461

NHT neointimal hyperplasia thickness, *NHA* neointimal hyperplasia area, *TASS* time-average shear stress, *TASSG* time-average shear stress gradient, *Combined_d* = log (TASS/(PlaqueArc + 1)) and *combined_m* = log (TASS* (PlaqueArc + 1))

method [8], the stented main vessel and its SB were reconstructed by the fusion of OCT and angiography and took the flow separation through SB into account, thus enabling accurate estimation of hemodynamics in bifurcations. The study observed an inverse association between baseline SS and neointimal response for struts located at bifurcated segments, assessed either as dichotomous coverage (yes vs. no) at 1-month follow-up or as neointimal area at 2-years follow-up. Those observations were consistent with previous evidence pointing out that low ESS promotes neointimal growth after BRS implantation [4]. Besides, it was observed the absolute magnitude of SS and gradient were significantly higher on jailing struts than on well-apposed struts. The mechanism may be explained by their exposure to high velocity flow and to the flow disturbances induced by the presence of the jailing struts themselves. This is also consistent with previous DES studies, demonstrating that struts detached from the vessel wall induce flow disturbances and higher SS rates [20].

Finally, previous studies have focused solely on hemodynamical factors, isolating their effect and disregarding potential interactions with other biological variables on the stent healing processes. Multiple factors, like plaque composition, inflammation, lesion complexity or the magnitude of tissue insult are also known to modulate the healing processes [6, 21]. It was shown that the combination of SS with IVUS-defined plaque characteristics had incremental value in predicting plaque progression and vulnerability [22]. Our systematic analysis of plaque characteristics (plaque arc degree and components) and their interaction with SS showed that the arc of plaque at baseline was associated with NTA at 2-year follow-up. Moreover, the combination of plaque arc degree and SS in the form of log (TASS/(PlaqueArc + 1)) had stronger correlation with NTA than SS alone in both core and non-core segments. This positive finding encourages future studies to address specifically the complex interactions between the abovementioned factors, which are of major importance to properly understand this complex phenomenon. Meanwhile, it was observed that segments with calcium plaque had significantly higher NHA and maximum NHT. This observation was contrary to previous findings in BMS and DES, where calcium induced less or had no impact on neointimal proliferation [5]. The discrepancy may be attributed to different operation procedures and mechanical interactions between calcium plaque and the stent. The radial strength of BRS is weaker than in BMS or DES, and the stiffness of calcium may cause stent deformation or even fractures [23], and thereby increases the degree of arterial injury that induces substantial local inflammation, which stimulates vascular smooth muscle cell proliferation and extracellular matrix deposition, resulting in neointimal thickening [1]. It is further speculated that, in order to reduce procedural complication, BMS and DES rather than BRS are optimal options for treatment of heavily calcified coronary lesions which are likely to generate a greater resistance to vessel opening [24] and increase the risk of fatigue fracture [23].

Characterization of the neointimal healing processes after stenting is methodologically very challenging. It requires the integration of multiple variables including time-consuming accurate biomechanical analysis of data from many patients. Still, the several million annual PCI procedures and the detrimental effects seen with treatment failure justifies the efforts to ensure more objective characterization of stent implants rather subjectively-guided intervention based on the intuition and experience of each operator, which is the present standard in most centres. This scenario might improve if the different modulating factors of the neointimal healing were better known, but we are still quite far from a biomechanically-guided optimization. Nonetheless, our study makes a significant step forward unravelling the interaction between intracoronary hemodynamics and the underlying plaque. Further studies are certainly warranted.

Limitations

One limitation of this study is that post-procedural OFDI images instead of pre-procedural images were used for baseline plaque characteristics quantification. However, due to the translucency of the material (Poly-L-lactic acid) of the DESolve BRS, there was no shadow behind struts, making the plaque analysis possible. Nevertheless, it should still be noted that plaque morphology may change due to the squeezing of plaque components during PCI and may not be exactly the same as pre-PCI. Another limitation is that our study investigated a single type of BRS. Nevertheless, the findings of the present study warrant additional prospective explorations of other types of BRS and investigation of more complex interactions between plaque property and hemodynamics that may influence stent healing processes.

Conclusion

In this serial analysis of neointimal healing after BRS implantation, it was found that intracoronary hemodynamics was associated with neointimal response for both bifurcation and non-bifurcation segments. Underlying plaque characteristics also played a role in stent healing and its interaction with shear stress was better correlated with neointimal hyperplasia area at 2-year follow-up. Investigating strategies of characterizing and optimizing local hemodynamics during stent implantation may be justified.

Funding The study was supported by the Natural Science Foundation of China (Grant No. 81871460) and Program of Shanghai Technology Research Leader.

Compliance with ethical standards

Conflict of interest Yingguang Li is employed by Medis medical imaging systems bv and has a research appointment at the Leiden University Medical Center (LUMC). Shengxian Tu received a research grant from Medis medical imaging and Pulse medical imaging technology, and Niels R. Holm received research grants from Medis medical imaging, Abbot, and Boston Scientific. All other authors declare that they have no conflict of interest.

References

1. Inoue T, Croce K, Morooka T, Sakuma M, Node K, Simon DI (2011) Vascular inflammation and repair: implications for re-endothelialization, restenosis, and stent thrombosis. J Am Coll Cardiol Interv 4:1057–1066
2. Brugaletta S, Radu MD, Garcia-Garcia HM et al (2012) Circumferential evaluation of the neointima by optical coherence tomography after ABSORB bioresorbable vascular scaffold implantation: can the scaffold cap the plaque? Atherosclerosis 221:106
3. Shishido K, Antoniadis AP, Takahashi S et al (2016) Effects of low endothelial shear stress after stent implantation on subsequent neointimal hyperplasia and clinical outcomes in humans. J Am Heart Assoc 5:e002949
4. Bourantas CV, Papafaklis MI, Kotsia A et al (2014) Effect of the endothelial shear stress patterns on neointimal proliferation following drug-eluting bioresorbable vascular scaffold implantation: an optical coherence tomography study. J Am Coll Cardiol Interv 7:315–324
5. Shimada Y, Kataoka T, Courtney BK et al (2006) Influence of plaque calcium on neointimal hyperplasia following bare metal and drug-eluting stent implantation. Catheter Cardiovasc Interv 67:866–869
6. Farb A, Weber DK, Kolodgie FD, Burke AP, Virmani R (2002) Morphological predictors of restenosis after coronary stenting in humans. Circulation 105:2974–2980
7. Holck EN, Fox-Maule C, Barkholt TØ et al (2019) Procedural findings and early healing response after implantation of a self-apposing bioresorbable scaffold in coronary bifurcation lesions. Int J Cardiovasc Imaging. https://doi.org/10.1007/s10554-019-01537-5
8. Li Y, Gutiérrez-Chico JL, Holm NR et al (2015) Impact of side branch modeling on computation of endothelial shear stress in coronary artery disease: coronary tree reconstruction by fusion of 3D angiography and OCT. J Am Coll Cardiol 66:125–135
9. Tu S, Barbato E, Köszegi Z et al (2014) Fractional flow reserve calculation from 3-dimensional quantitative coronary angiography and TIMI frame count: a fast computer model to quantify the functional significance of moderately obstructed coronary arteries. J Am Coll Cardiol Interv 7:768–777
10. van Ditzhuijzen NS, Karanasos A, Bruining N et al (2014) The impact of Fourier-Domain optical coherence tomography catheter induced motion artefacts on quantitative measurements of a PLLA-based bioresorbable scaffold. Int J Cardiovasc Imaging 30:1013–1026
11. Nakatani S, Sotomi Y, Ishibashi Y et al (2016) Comparative analysis method of permanent metallic stents (XIENCE) and bioresorbable poly-L-lactic (PLLA) scaffolds (Absorb) on optical coherence tomography at baseline and follow-up. EuroIntervention 12:1498–1509
12. Tearney GJ, Regar E, Akasaka T et al (2012) Consensus standards for acquisition, measurement, and reporting of intravascular optical coherence tomography studies: a report from the International Working Group for Intravascular Optical Coherence Tomography Standardization and Validation. J Am Coll Cardiol Interv 59:1058–1072
13. Wentzel JJ, Krams R, Schuurbiers JC et al (2001) Relationship between neointimal thickness and shear stress after Wallstent implantation in human coronary arteries. Circulation 103:1740–1745
14. Gijsen FJ, Oortman RM, Wentzel JJ et al (2003) Usefulness of shear stress pattern in predicting neointima distribution in sirolimus-eluting stents in coronary arteries. Am J Cardiol 92:1325–1328
15. Papafaklis MI, Bourantas CV, Theodorakis PE et al (2010) The effect of shear stress on neointimal response following sirolimus- and paclitaxel-eluting stent implantation compared with bare-metal stents in humans. J Am Coll Cardiol Interv 3:1181–1189
16. Suzuki N, Nanda H, Angiolillo DJ et al (2008) Assessment of potential relationship between wall shear stress and arterial wall response after bare metal stent and sirolimus-eluting stent implantation in patients with diabetes mellitus. Int J Cardiovasc Imaging 24:357–364
17. Li Y, Li Z, Holck EN et al (2018) Local flow patterns after implantation of bioresorbable vascular Scaffold in coronary bifurcations—novel findings by computational fluid dynamics. Circ J 82:1575–1583
18. Thondapu V, Tenekecioglu E, Poon EK et al (2018) Endothelial shear stress 5 years after implantation of a coronary bioresorbable scaffold. Eur Heart J 39:1602–1609
19. Bourantas CV, Papafaklis MI, Lakkas L et al (2014) Fusion of optical coherence tomographic and angiographic data for more accurate evaluation of the endothelial shear stress patterns and neointimal distribution after bioresorbable scaffold implantation: comparison with intravascular ultrasound-derived reconstructions. Int J Cardiovasc Imaging 30:485–494
20. Foin N, Gutiérrez-Chico JL, Nakatani S et al (2014) Incomplete stent apposition causes high shear flow disturbances and delay in neointimal coverage as a function of strut to wall detachment distance: implications for the management of incomplete stent apposition. Circ Cardiovasc Interv 7:180–189
21. Koskinas KC, Chatzizisis YS, Antoniadis AP, Giannoglou GD (2012) Role of endothelial shear stress in stent restenosis and thrombosis: pathophysiologic mechanisms and implications for clinical translation. J Am Coll Cardiol 59:1337–1349
22. Corban MT, Eshtehardi P, Suo J et al (2014) Combination of plaque burden, wall shear stress, and plaque phenotype has incremental value for prediction of coronary atherosclerotic plaque progression and vulnerability. Atherosclerosis 232:271–276
23. Halwani DO, Anderson PG, Brott BC, Anayiotos AS, Lemons JE (2012) The role of vascular calcification in inducing fatigue and fracture of coronary stents. J Biomed Mater Res B 100:292–304
24. Morlacchi S, Pennati G, Petrini L, Dubini G, Migliavacca F (2014) Influence of plaque calcifications on coronary stent fracture: a numerical fatigue life analysis including cardiac wall movement. J Biomech 47:899–907